Astron. Astrophys. 325, 352–359 (1997)

ASTRONOMY
AND
ASTROPHYSICS

Vertical prominence oscillations and stability

A comparison of the influence of the distant photosphere in Inverse Polarity and Normal Polarity prominence models

N.A.J. Schutgens

Sterrekundig Instituut Utrecht, Utrecht University, Postbus 80.000, 3508 TA Utrecht, The Netherlands

Received 16 January 1997 / Accepted 24 March 1997

Abstract. All MHD models for prominence equilibrium to date can, in essence, be reduced to two simple current models that describe so-called Inverse (IP) and Normal (NP) Polarity topologies. Using these simple current models, I investigate the influence of the boundary condition provided by the distant photosphere (flux conservation) on vertical prominence oscillations.

The fact that the photosphere is some distance z away from the prominence, implies that the Lorentz force acting on the prominence, due to the photospheric boundary condition, evolves with a delay $z/v_{\rm A}$ ($v_{\rm A}$: coronal Alfvénspeed).

In an earlier paper (Schutgens 1997), it was shown that, in the case of a Kuperus-Raadu (IP) prominence, this delay can greatly influence the vertical stability properties of prominences, especially when $\omega\tau_0 \gtrsim 1$ (ω: frequency of oscillation, $\tau_0 = 2z/v_{\rm A}$).

In this paper a comparative study is made of this effect in IP and NP prominences.

Because of a different force balance, NP and IP prominences have currents and oscillation periods of different magnitude. The influence of the distant photosphere on NP prominences is minimal, while it has a very pronounced effect on IP prominences. As a result, NP and IP prominences have widely different stability properties. Foot point shaking due to photospheric 5 min. oscillations will only excite IP prominences.

Key words: Sun: prominences – Sun: oscillations – magnetic fields – waves

1. Introduction

For the past 50 years a variety of oscillatory modes have been observed in prominences (Vrsnak & Ruzdjak, 1994). Spectral analysis of limb prominences shows horizontal oscillations (see Tsubaki 1988 for a review), while vertical oscillations can be seen in disk filaments (Thompson & Schmieder 1991, Yi Zhang et al. 1991, Yi Zhang & Engvold 1991).

The horizontal oscillations can be grouped in short period (3–8 min.) and long period (40–80 min.) oscillations, both with velocity amplitudes of about 2 km/s. Recently also sub-minute oscillations were detected (Balthasar et al. 1993). The vertical oscillations have periods of 2.5–16 min. with somewhat smaller velocity amplitudes. As the observations of the vertical oscillations were done with 2D-spectral scans, they also yielded information on the spatial structures that oscillate. Yi Zhang et al. (1991) showed that the oscillations were confined to thread-like structures within the prominence. It is well possible that these structures are related to the filament fine structure, which consists of fibrils, 300–1000 km in diameter, that contain most of the prominence matter (Schmieder 1988, 1992).

Hyder (1966) and Kleczek & Kuperus (1969) offered the first models for oscillations of so-called 'winking' filaments (Ramsey & Smith 1966). Later Oliver et al. (1992, 1993), Oliver & Ballester (1995, 1996), Joarder & Roberts (1992, 1993) and Joarder et al. (1997) formulated MHD models for prominence oscillations. For typical prominence parameters these models all predict periods as are observed in real prominences.

Recently the influence of the photosphere on prominence dynamics was investigated in more detail by van den Oord & Kuperus (1992) and Schutgens (1997). The photosphere can, indirectly, support a prominence against gravity (Kuperus & Raadu 1974). Essentially, the photosphere provides a boundary condition (constant magnetic flux) at a certain distance z from the main prominence body. The current running through the prominence body creates a field that cannot enter the photosphere. The repulsion of the prominence field by the photosphere results in an upward Lorentz force on the prominence body. However, this boundary condition is conveyed to the prominence on a timescale $\frac{1}{2}\tau_0 = z/v_{\rm A}$ ($v_{\rm A}$: Alfvénspeed). In time-dependent situations the upward, supporting force experiences a delay $z/v_{\rm A}$ in its evolution as compared to the other acting forces. Schutgens (1997, hereafter: Paper I) found that the stability properties of prominence oscillations are strongly influenced by these delays.

Send offprint requests to: Nick Schutgens

Their influence becomes dominant when $\omega\tau_0 \gtrsim 1$, where ω is the frequency of oscillation.

Oliver et al. (1992, 1993), Oliver & Ballester (1995, 1996), Joarder & Roberts (1992, 1993) and Joarder et al. (1997) use a fundamentally different model for prominence equilibrium than van den Oord & Kuperus (1992) and Schutgens (1997). The first group of authors use Kippenhahn-Schlüter (KS) equilibria (Kippenhahn & Schlüter 1957), while the other authors employed a Kuperus-Raadu (KR) equilibrium (Kuperus & Raadu 1974). It was surmised in Paper I that the effects of delayed prominence – photosphere 'communication' are only important for KR prominences as they are solely supported by photospheric flux conservation. KS prominences would behave quite differently.

Comparative studies of the vertical stability of KS- and KR-type prominences have been made by Amari & Aly (1989), Démoulin & Priest (1988), Ridgway et al. (1991) and Démoulin et al. (1991) (see also Anzer & Ballester 1990). These authors model the prominence as an infinitely thin wire or slab located in a force-free field and then perform a *quasi-stationary* stability analysis. Démoulin & Priest and Démoulin et al. show that both types can suffer a van Tend-Kuperus kind of instability (van Tend & Kuperus 1978), but that KR prominences are more prone to it.

When one views a prominence as a mass loaded current, embedded in a coronal arcade, both the KS and KR equilibria can be described by a similar force balance (see Sect. 2 and also Priest 1990, p. 150). In KS prominences the Lorentz force due to the magnetic arcade is directed upwards and supports the prominence against gravity. In KR prominences this Lorentz force is directed downwards and only photospheric flux conservation prevents the prominence from falling down. This basic difference leads to completely different field topologies (see also Fig. 2) that are nowadays described as Inverse Polarity and Normal Polarity topologies. A KS model gives rise to a NP topology, a KR model to an IP topology. Leroy et al. (1984) showed that the majority of observed prominences and all polar crown prominences have an Inverse Polarity topology, while the rest has a Normal Polarity topology.

This paper is structured as follows. In Sect. 2 I discuss equilibria of NP and IP prominences. Then, in Sect. 3, the NP and IP equilibrium models will be extended to time dependent situations, using the mathematical formalism developed in Paper I. Prominence oscillations in both NP and IP configurations are studied and compared. Finally Sect. 4 contains a summary and the conclusions. All dimensional quantities in this paper are in rational MKSA units.

2. Field topology and prominence equilibrium

The prominence is modelled as a mass loaded wire current $I_0 > 0$ hanging above the photosphere at height z. The repelling force due to photospheric flux conservation can be calculated by introducing a mirror current $-I_0$ at a depth $-z$ (Kuperus & Raadu 1974, van Tend & Kuperus 1978). In the mathematical description of the system, this mirror current replaces the photospheric boundary condition. Hence the upward force due to flux conservation becomes $I_0 B_{\rm mir} = \mu_0 I_0^2/4\pi z$. In addition there is another Lorentz force due to the coronal arcade $B_{\rm cor}(z)$ and of course the gravitational force $mg(z)$. Here, m is the prominence mass line density (in the longitudinal direction). Prominence equilibrium per unit length is determined by a balance of these forces:

$$F_{\rm stat}(z) = I_0\,(B_{\rm mir}(z) + B_{\rm cor}(z)) - mg(z) = 0. \tag{1}$$

With $g, B_{\rm mir} > 0$, $B_{\rm cor}$ can be either positive or negative. IP models have $B_{\rm cor} < 0$, while NP models assume $B_{\rm cor} > 0$. The equilibrium current is

$$I_0 = -\frac{2\pi z B_{\rm cor}(z)}{\mu_0} + \sqrt{\left(\frac{2\pi z B_{\rm cor}(z)}{\mu_0}\right)^2 + \frac{4\pi m z g(z)}{\mu_0}}. \tag{2}$$

There is of course another solution with $I_0 < 0$, but this does not lead to new field topologies. For a potential arcade $B_{\rm cor} = B_0 {\rm e}^{-z/H}$ ($H = 10^5$ km), a range of prominence mass line densities m and arcade field strengths B_0, the equilibrium current is plotted as a function of height in Fig. 1. For the gravitational acceleration g, the full functional form ($\sim 1/r^2$) is used.

Below $z = 10^6$ km, IP and NP prominences behave distinctly different, as long as the arcade field strength B_0 is not too small. The currents in IP prominences are typically one or more magnitudes larger than in their NP counterparts (see also Démoulin & Priest 1988). The IP equilibrium is completely determined by the balance of magnetic forces, gravity is negligible. The NP equilibrium on the other hand, is a balance between the magnetic forces and gravity. Below $z = 10^5$ km, the effect of photospheric flux conservation in NP configurations is small and gravity is mainly balanced by the Lorentz force due to the arcade. Note that in case the arcade field strength is very weak ($B_0 = 10^{-4}$ T) there is little difference between IP and NP prominences, as is expected.

Above $z = 10^6$ km, the arcade field becomes too weak. Equilibrium is determined by photospheric flux conservation and gravity. There is no clear distinction between the IP and NP force balance. Note that quiescent prominences are usually located between 10 000 and 50 000 km.

Each curve for the equilibrium current as a function of height has its own maximum. For the IP configuration with a sufficiently large arcade field strength $B_0 \gtrsim 10^{-3}$ T, this maximum current corresponds to the van Tend-Kuperus instability (van Tend & Kuperus 1978) that can give rise to two ribbon flares (Kaastra 1985, Martens & Kuin 1989). Apparently an instability also exists for NP prominences (see also Démoulin & Priest 1988). This results solely from the inclusion of photospheric flux conservation effects in NP configurations. Note that, as the currents are larger, much more energy can be stored in an IP prominence than in a NP prominence.

In Fig. 2, I have plotted the field lines for NP and IP prominences. In both cases, the magnetic field is the sum of the field of two infinite and straight wire currents (prominence and mirror

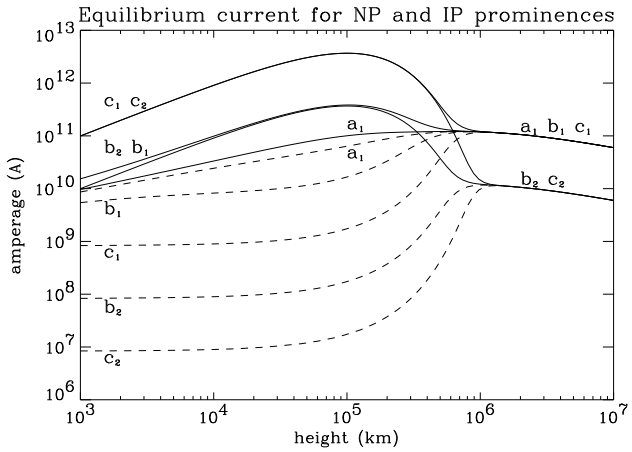

Fig. 1. The equilibrium current for NP (dashed lines) and IP (solid lines) prominences as a function of height. The prominence is located in a magnetic arcade with $H = 10^5$ km. a_1: $m = 3.1 \times 10^4$ kg/m, $B_0 = 10^{-4}$ T; b_1: $m = 3.1 \times 10^4$ kg/m, $B_0 = 10^{-3}$ T; b_2: $m = 3.1 \times 10^2$ kg/m, $B_0 = 10^{-3}$ T; c_1: $m = 3.1 \times 10^4$ kg/m, $B_0 = 10^{-2}$ T; c_2: $m = 3.1 \times 10^2$ kg/m, $B_0 = 10^{-2}$ T.

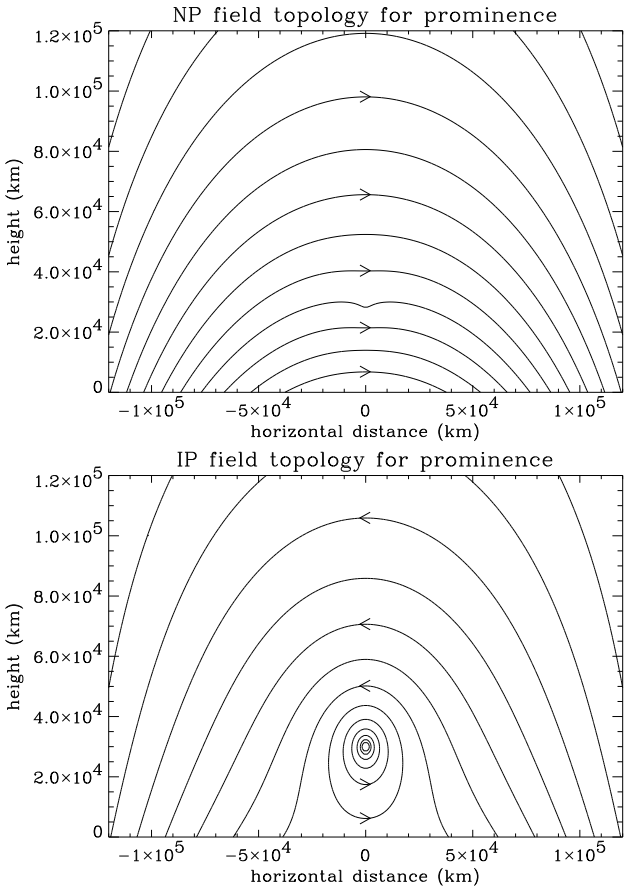

Fig. 2. Field lines in a NP and IP configuration. Parameters for the prominence are $z = 3 \times 10^4$ km, $m = 3.1 \times 10^4$ kg/m, $B_0 = 10^{-3}$ T, $H = 10^5$ km. Top picture: NP configuration, $I_0 = 9.9 \times 10^9$ A. Bottom picture: IP configuration, $I_0 = 2.3 \times 10^{11}$ A.

current) and a potential arcade. The magnetic arcade is clearly visible in both plots. In the NP configuration the field lines deviate only mildly from that of the potential arcade. The prominence body is located in the small dip in the field lines at height $z = 3 \times 10^4$ km. This dip provides the necessary magnetic tension to support the prominence mass against gravity. In the IP configuration the strong current at the location of the prominence body can be seen. The prominence mass 'rests' on its own field, which cannot enter the photosphere (flux conservation). The location of the prominence is an O-type neutral point for both NP and IP prominences (for NP prominences the scale of Fig 2 is too large to show this). Just *above* the NP prominence, an X-type neutral point can form as the horizontal field component rapidly changes sign with height. For IP prominences it is known (e.g. Kaastra 1985) that an X-type neutral point can form *below* the prominence as it rises. Such X-type neutral points are necessary to liberate the prominence from the overlying arcade during an eruption. Note that, due to the Lorentz force, the arcade stabilizes the current in an IP topology against horizontal perturbations, while in the NP case the prominence is horizontally unstable (van Tend & Kuperus 1978, Drake et al. 1993).

In the quasi-stationary approximation for the field evolution, one can easily determine the oscillation frequency $\omega_{\rm stat}$ from the equation of motion. Given the equilibrium of Eq. (1),

$$\omega_{\rm stat}^2 = -\frac{1}{m}\frac{\partial F_{\rm stat}}{\partial z} = \frac{\mu_0}{4m\pi}\frac{I_0^2}{z^2} + \frac{I_0 B_0}{mH}\mathrm{e}^{-z/H} - \frac{2GM_\odot}{(R_\odot + z)^3} \quad (3)$$

Fig. 3 shows the quasi-stationary eigenperiods of NP and IP prominences with different mass line densities m and arcade field strengths B_0. For typical quiescent prominence heights, IP configurations have much shorter eigenperiods than NP configurations. Also, they show a completely different dependence on prominence mass line density and arcade field strength. The instability mentioned when discussing Fig. 1, shows up as vertical asymptotes. Here the squared eigenfrequency $\omega_{\rm stat}^2$ becomes negative and the solution grows exponentially.

3. Oscillations of IP and NP prominences

A consistent treatment of global prominence oscillations can not be based on the quasi-stationary approximation, but includes the dynamical field evolution instead. This comes down to solving Maxwell's equations for a moving mirror current. Field changes at the location of the mirror current take at least a time $\tau_0 = 2z_0/v_{\rm A}$ to propagate to the prominence current. In particular, these travel times range from $2z_0/v_{\rm A}$ to infinity (see Paper I). This is typical for waves generated by two-dimensional sources (Morse & Feshbach 1963, p. 834).

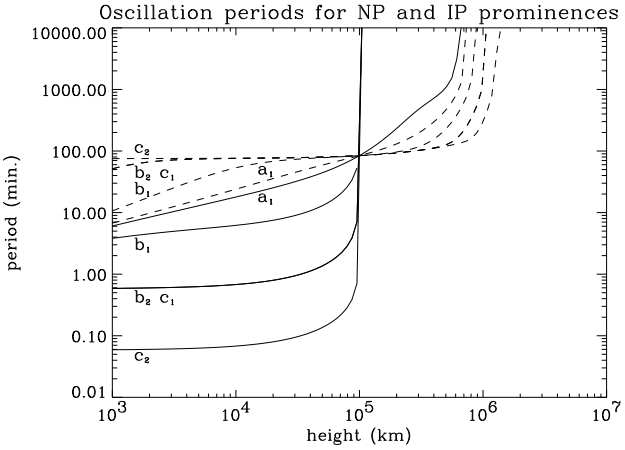

Fig. 3. Oscillation periods for NP (dashed lines) and IP (solid lines) prominences as a function of height. The prominence is located in a magnetic arcade with $H = 10^5$ km. a_1: $m = 3.1\times10^4$ kg/m, $B_0 = 10^{-4}$ T; b_1: $m = 3.1 \times 10^4$ kg/m, $B_0 = 10^{-3}$ T; b_2: $m = 3.1 \times 10^2$ kg/m, $B_0 = 10^{-3}$ T; c_1: $m = 3.1\times10^4$ kg/m, $B_0 = 10^{-2}$ T; c_2: $m = 3.1\times10^2$ kg/m, $B_0 = 10^{-2}$ T.

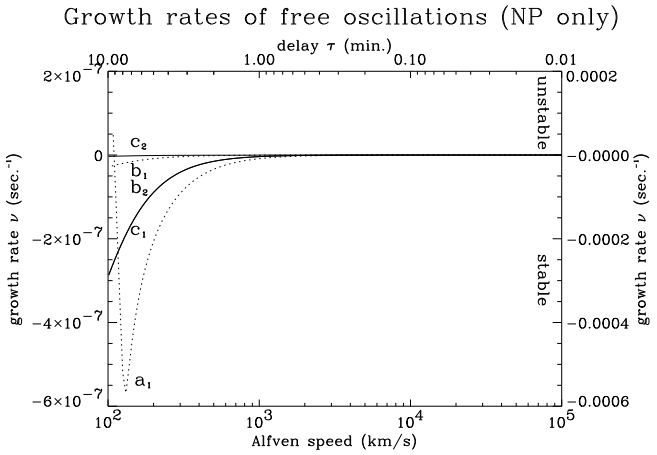

Fig. 4. The growth rates of NP prominence oscillations as a function of Alfvénspeed. The scalebar for the solid lines (b_2, c_1, c_2) is on the left y-axis, the scalebar for the dotted lines (a_1, b_1) is on the right y-axis. The prominence is located at a height z = 30 000 km in an arcade with H = 100 000 km. Notice that the curves for b_2 and c_1 coincide. a_1) $m = 3.1\times10^4$ kg/m, $B_0 = 10^{-4}$ T; b_1) $m = 3.1\times10^4$ kg/m, $B_0 = 10^{-3}$ T; c_1) $m = 3.1 \times 10^4$ kg/m, $B_0 = 10^{-2}$ T. b_2) $m = 3.1 \times 10^2$ kg/m, $B_0 = 10^{-3}$ T; c_2) $m = 3.1 \times 10^2$ kg/m, $B_0 = 10^{-2}$ T.

In Paper I an equation of motion was derived. Using the dimensionless quantities

$$t = \sqrt{\tfrac{\mu_0 m}{4\pi}}\tfrac{1}{B_0}\tilde{t}, \quad I_0 = \tfrac{4\pi}{\mu_0} z_0 B_0 \tilde{I}_0, \quad \nu_{\rm ph} = \sqrt{\tfrac{4\pi m}{\mu_0}} B_0 \tilde{\nu}_{\rm ph},$$
$$z = z_0\tilde{z}, \quad x = z_0\tilde{x}, \quad \chi = \tfrac{z_0}{H_0} \quad \tau_0 = 2\tfrac{z_0}{v_{\rm A}} B_0 \sqrt{\tfrac{4\pi}{\mu_0 m}},$$
$$\text{and} \quad \gamma = \tfrac{2\mu_0 G M_\odot m}{\pi z_0 B_0^2 R_\odot^2} \quad \tilde{g}(\tilde{z}) = \tfrac{1}{8}\gamma \tfrac{1}{(1+\tilde{z}_0/\tilde{R}_\odot)^2},$$

this equation of motion can be written (drop the tildes):

$$\ddot{z}(t) = F(z) = I_0 \left\{ B_{\rm mir}(t,z) + \sigma e^{-\chi z(t)} \right\} - \nu_{\rm ph}\dot{z}(t) - g(z) \quad (4)$$

with $\sigma = +1$ for NP prominences and $\sigma = -1$ for IP prominences. The force term in this equation of motion resembles the force term in Eq. (1), but the term $B_{\rm mir}$ now contains the dynamical field evolution. The field of the mirror current is given by (Paper I)

$$B_{\rm mir}(t,z) = I_0 \int_0^\infty dx' \frac{1}{F_{t'}^2 R_{t'}^2} \left[\frac{2(z(t)+z(t'))}{F_{t'} R_{t'}} + \tau_0 \frac{\dot{z}(t')}{F_{t'}} - \tau_0^2 \frac{(z(t)+z(t'))^2 \ddot{z}(t')}{2F_{t'} R_{t'}} \right]_{t-t'=\tau_0 R_{t'}/2}, \quad (5)$$

with $R_{t'} = \sqrt{x'^2 + (z(t)+z(t'))^2}$ and $F_{t'} = 1 + \frac{1}{2}\tau_0 \frac{z(t)+z(t')}{R_{t'}} \dot{z}(t')$. The prominence and mirror currents are located in the $y = 0$ plane, parallel to the x-axis. The prominence current is at a height $z(t)$, the mirror current at a depth $-z(t)$. The dimensionless Alfvénspeed equals $2/\tau_0$. For $\tau_0 \to 0$, the field of the mirror current reduces to the quasi-stationary approximation. Equation (4) is a so-called differential equation with delays (see Saaty 1981 for an introduction).

Following Paper I, I also included a phenomenological damping term ($\nu_{\rm ph}$). This physical damping can be attributed to a variety of mechanisms: mass friction (Hyder 1966), emission of sound waves (Kleczek & Kuperus 1969) and emission of Alfvénwaves (van den Oord & Kuperus 1992). As its numerical value is uncertain (see also Paper I), the computations presented in this paper were all done with $\nu_{\rm ph} = 0$.

Note that, under the assumption $\nu_{\rm ph} = 0$, any *dimensional* time scale one can possibly derive from the equation of motion depends only on $B_0/\sqrt{m}$, not on B_0 or m separately.

An approximate solution to the equation of motion, valid for small amplitude oscillations, was derived in Paper I. In general this solution consists of an infinite series of harmonic oscillations $e^{s_k t}$ with complex frequency s_k, $k = 0, 1, 2, 3, \ldots$. These complex frequencies are solutions of the characteristic equation

$$h(s) \equiv s^2 + \nu_{\rm ph} s - \frac{1}{2}\tau_0^2 s^2 I_0^2 K_1'(\tau_0 s) + \omega_{\rm stat}^2 - \frac{1}{2} I_0^2 = 0 \quad (6)$$

where $\omega_{\rm stat}$ is the oscillation frequency in the quasi-stationary approximation and K_1 is the modified Bessel function of the second kind, of order 1 (Abramowitz & Stegun 1968, Ch. 9). The accent denotes differentiation with respect to the argument.

Each zero s_k can be written as $s_k = \nu_k + i\omega_k$ with growth rate $\nu_k \in \mathbb{R}$ and frequency $\omega_k \in \mathbb{R}$. The s_k can be ordered according to decreasing (!) real part ($\nu_0 \geq \nu_1 \geq \nu_2 \geq \cdots$). If $\nu_0 > 0$ the solution grows in time and is unstable. For $\nu_0 < 0$ the solution is stable. Usually oscillations belonging to the s_k with the lowest k's dominate the solution, as the amplitudes decrease with increasing k. There is an infinite number of zeroes s_k, but only a finite number of zeroes with $\nu_k > \alpha$, $\forall\, \alpha \in \mathbb{R}$. Usually

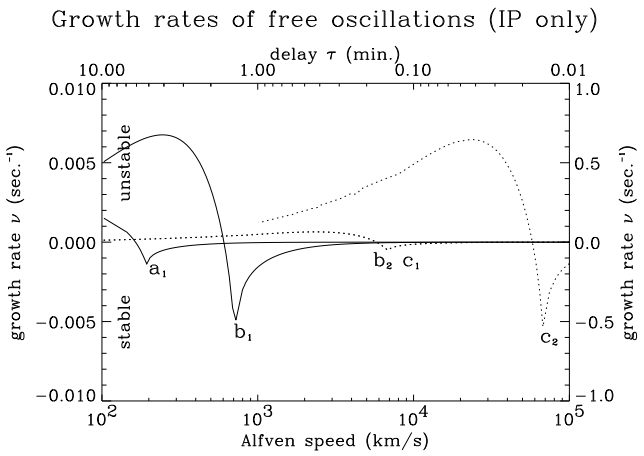

Fig. 5. The growth rates of IP prominence oscillations as a function of Alfvénspeed. The scalebar for the solid lines (b_2, c_1, c_2) is on the left y-axis, the scalebar for the dotted lines (a_1, b_1) is on the right y-axis. The prominence is located at a height z = 30 000 km in an arcade with H = 100 000 km. The growth rate for the prominence labelled c_2 could not be computed reliably for $v_A \in [100, 1000]$ km/s. Notice that the curves for b_2 and c_1 coincide. a_1) $m = 3.1 \times 10^4$ kg/m, $B_0 = 10^{-4}$ T; b_1) $m = 3.1 \times 10^4$ kg/m, $B_0 = 10^{-3}$ T; c_1) $m = 3.1 \times 10^4$ kg/m, $B_0 = 10^{-2}$ T. b_2) $m = 3.1 \times 10^2$ kg/m, $B_0 = 10^{-3}$ T; c_2) $m = 3.1 \times 10^2$ kg/m, $B_0 = 10^{-2}$ T.

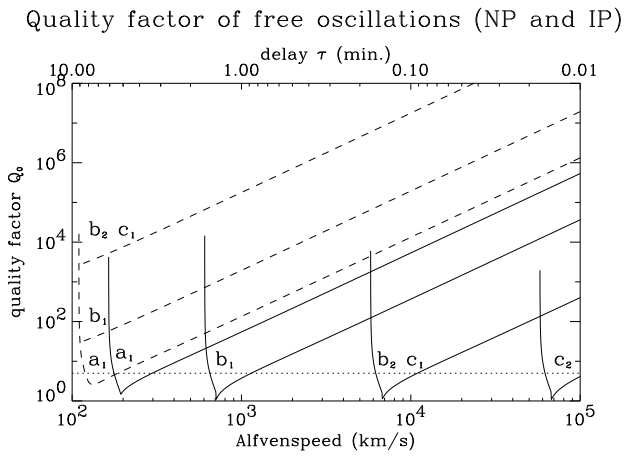

Fig. 6. The quality factors of stable (!) IP (solid line) and NP (dashed line) prominence oscillations as a function of Alfvénspeed. The prominence is located at a height z = 30 000 km in an arcade with H = 100 000 km. Notice that the curves for b_2 and c_1 coincide. The dotted line is given by $Q_0 = 5$. a_1) $m = 3.1 \times 10^4$ kg/m, $B_0 = 10^{-4}$ T; b_1) $m = 3.1 \times 10^4$ kg/m, $B_0 = 10^{-3}$ T; c_1) $m = 3.1 \times 10^4$ kg/m, $B_0 = 10^{-2}$ T. b_2) $m = 3.1 \times 10^2$ kg/m, $B_0 = 10^{-3}$ T; c_2) $m = 3.1 \times 10^2$ kg/m, $B_0 = 10^{-2}$ T.

all zeroes are simple. As both s_k and its complex conjugate are zeroes of $h(s)$, I only consider $\omega_k > 0$ in the remainder of this paper.

In Paper I, a code named ROOTS is described that can search for the zeroes s_k in a designated part of the complex plane. In this paper, I used this code to compute s_0 for a range of IP and NP prominences.

First of all I compare the influence of delayed boundary conditions on IP and NP prominences by studying oscillation growth rates as a function of the Alfvénspeed. The prominence, with mass line density m, is assumed to be at a height z_0 = 30 000 km in a magnetic arcade with arcade field strength B_0 and H = 100 000 km . The results are shown in Figs. 4 and 5. The growth rate approximates zero for large Alfvénspeeds as the quasi-stationary solution is marginally stable. Apparently, this quasi-stationary approximation is valid for NP prominences for the plotted range of Alfvénspeeds. The delays do not seem to influence the stability of NP prominences. The IP prominences, on the other hand, are strongly influenced by delays. With increasing τ_0 (decreasing Alfvénspeeds) the oscillations first become more strongly damped (see also Fig. 6), and finally stability is lost. Instability occurs for $\omega_0 \tau_0 \gtrsim 1$ (compare Fig. 3 and Fig. 5). This was also found in Paper I. Note again that for weak arcade field strength ($B_0 = 10^{-4}$ T), the difference between IP and NP vanishes.

For most values of v_A, for which an IP or NP prominence is stable, the zero s_0 dominates all other zeroes. Hence only one frequency (ω_0) is present and it is close to the quasi-stationary frequency ω_{stat}. Around the local minima in the damping rate, another frequency starts dominating just before instability sets in. Only then is there a significant change in the oscillation frequency, but not more than a factor 2.

The effect of retardation on IP and NP oscillations can also be analyzed using the quality factor $Q_0 = \omega_0 / 2\nu_0$. Fig. 6 shows that the oscillations in IP prominences become strongly damped for specific values of v_A, while in general NP prominences exhibit marginally stable oscillations (Q_0 changes over many magnitudes, even for NP prominences, but if one observes only for about 10 periods there is little difference between oscillations with $Q_0 = 10^2$ or $Q_0 = 10^8$). The only exception is the NP prominence located in a weak arcade $B_0 = 10^{-4}$ T, that shows behaviour similar to the IP prominences, as the mirror force is no longer dominated by the force due to the arcade.

Also, as follows from the results for IP prominences, the stronger the prominence current, the stronger the effects of delays. This confirms the surmise in Paper I that NP prominences are less affected by the distant photosphere than IP prominences due to the relatively weak mirror force.

Quiescent prominences usually float 30 000–50 000 km above the photosphere. For the same prominence mass line density m, a different equilibrium height is found for different values of the equilibrium current I_0. The oscillation periods and quality factors can be studied as a function of height. For this, I assumed an Alfvénspeed of 1000 km/s. In Fig. 7 the oscillation periods are shown. Heavy IP prominences in strong arcade fields (like the IP prominence labelled c_1 in previous plots) are unstable and thus ignored. In all cases the periods agree well with the quasi-stationary periods (less than 1% difference), with the exception of the IP prominence labelled b_1. For the latter, I plotted the quasi-stationary period as well. The

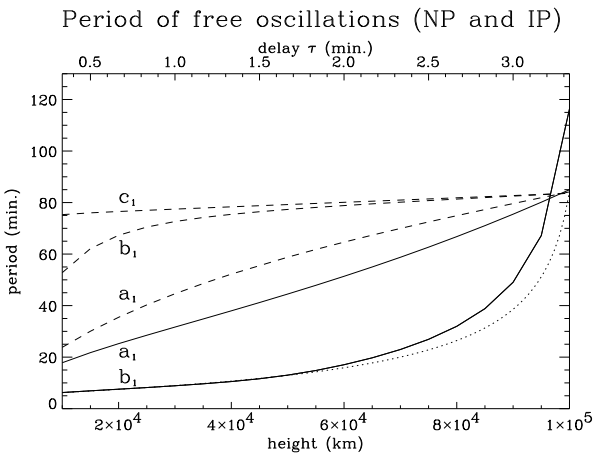

Fig. 7. The periods of prominence oscillations as a function of height. The IP (solid lines) and NP (dashed lines) prominences are located in an arcade with $H = 10^5$ km and $B_0 = 10^{-3}$ T. The Alfvénspeed is assumed $v_A = 1000$ km/s. The dotted line is the quasi-stationary period for the IP prominence labelled b_1. All other prominences have quasi-stationary periods that deviate less than 1% from the dynamical period. a_1) $m = 3.1 \times 10^4$ kg/m, $B_0 = 10^{-4}$ T; b_1) $m = 3.1 \times 10^4$ kg/m, $B_0 = 10^{-3}$ T; c_1) $m = 3.1 \times 10^4$ kg/m, $B_0 = 10^{-2}$ T. b_2) $m = 3.1 \times 10^2$ kg/m, $B_0 = 10^{-3}$ T; c_2) $m = 3.1 \times 10^2$ kg/m, $B_0 = 10^{-2}$ T.

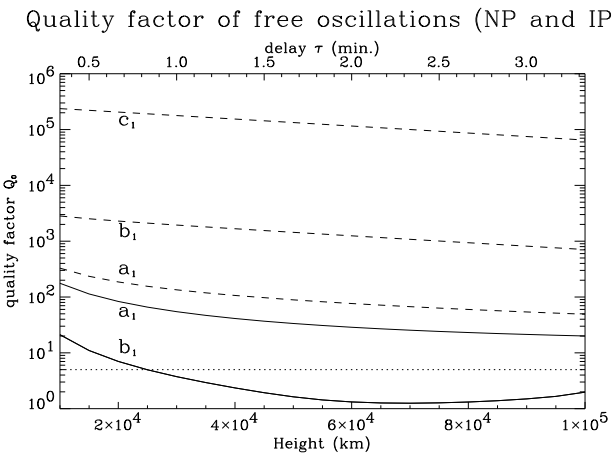

Fig. 8. The quality factors of prominence oscillations as a function of height. The IP (solid lines) and NP (dashed lines) prominences are located in an arcade with $H = 10^5$ km and $B_0 = 10^{-3}$ T. The Alfvénspeed is assumed $v_A = 1000$ km/s. The dotted line is given by $Q_0 = 5$. a_1) $m = 3.1 \times 10^4$ kg/m, $B_0 = 10^{-4}$ T; b_1) $m = 3.1 \times 10^4$ kg/m, $B_0 = 10^{-3}$ T; c_1) $m = 3.1 \times 10^4$ kg/m, $B_0 = 10^{-2}$ T. b_2) $m = 3.1 \times 10^2$ kg/m, $B_0 = 10^{-3}$ T; c_2) $m = 3.1 \times 10^2$ kg/m, $B_0 = 10^{-2}$ T.

two periods differ at most by 50%. The quality factors (Fig. 8) again confirm that NP prominences are well described using the quasi-stationary theory (which predicts marginally stable oscillations). But IP prominences can be strongly inhibited to oscillate or experience instability, depending on the delays.

Finally, I consider forced oscillations. It has been suggested that prominence oscillations of 3 and 5 min. are related to the chromospheric and photospheric periods. Given a driving frequency ω_d the equation of motion is now (in dimensional variables):

$$m\ddot{z} = F(z) + f_0 \cos \omega_d t.$$

One can substitute $z(t) = z_0 + h_0 \sin \omega_d t$ and look for solutions of the oscillation amplitude h_0 as a function of the mass line density m and the equilibrium height z_0. In the context of forced oscillations this amplitude h_0 is also known as the amplitude response function and if it is large, forcing is very efficient. In Paper I, this response function was shown to be proportional to $h^{-1}(\omega_d \tau_0 i)$.

Forced oscillations of 3 or 5 min. hardly excite NP prominences, their eigenperiods being one or two orders of magnitude larger than the driving periods. For IP prominences the eigenperiods and the driving periods can be of the same order, so excitation is more easily accomplished. Results for IP prominences in an arcade field $H = 100\,000$ km and $B_0 = 10^{-3}$ T are plotted in Fig. 9 for a driving period of 5 minutes. The six different graphs are for different values of the Alfvénspeed. The black areas are parameter regimes (z_0, m) where driving leads to growing oscillations (instability). In the remaining part of the graphs the response function $h^{-1}(\omega_d \tau_0 i)$ is plotted as a grayscale. The lighter the shade, the larger the response function. The thin black curve connects all prominences z_0, m that have a *quasi-stationary* eigenperiod of 5 minutes. The dashed white line connects all prominences z_0, m with $\omega_{stat} \tau_0 = 1$. For the chosen parameter regimes, the 'quasi-stationary' van Tend-Kuperus instability occurs if $z_0 > 10^5$ km.

For high Alfvénspeeds (Fig. 9, graph f), the results are almost identical to the quasi-stationary theory. Most prominences are stable and excitation of forced oscillations occurs only along the thin black curve. If the Alfvénspeed is lowered, the most notable change is that the parameter regime for unstable prominences grows. Hence one may conclude that retardation has, in general, a destabilizing effect. Apart from this little else seems to change. However, at some value of v_A a new excitation peak appears (the bright little dot on the border of the domain of instability of graphs a, b,c and d). It represents prominences whose dominating zero $s_0 = \omega_d i$ (marginally stable !). That is, their *dynamical* eigenperiod matches the driving period, and forcing is very efficient. For even lower Alfvénspeeds, prominences with $\omega_{stat} = \omega_d$ show less and less response to driving.

What is interesting about this new excitation peak is that it persists, near $\omega_0 \tau_0 = 1$ while $\omega_0 = \omega_d$, if a physical damping is introduced (in Fig. 9, $\nu_{ph} = 0$). Its position may shift in parameter space, like all other features, but there will always be a specific match of z_0 and m for which strong excitation results. Prominences with $\omega_{stat} = \omega_d$ are in their response very sensitive to damping. With *increased* damping ν_{ph}, the response *decreases* strongly. This is similar to the classic driven harmonic oscillator, whose amplitude decreases with increased damping (e.g. friction). Basically this means that only prominences that fulfill the condition $\omega_0 \tau_0 = \omega_d \tau_0 \approx 1$ will resonate.

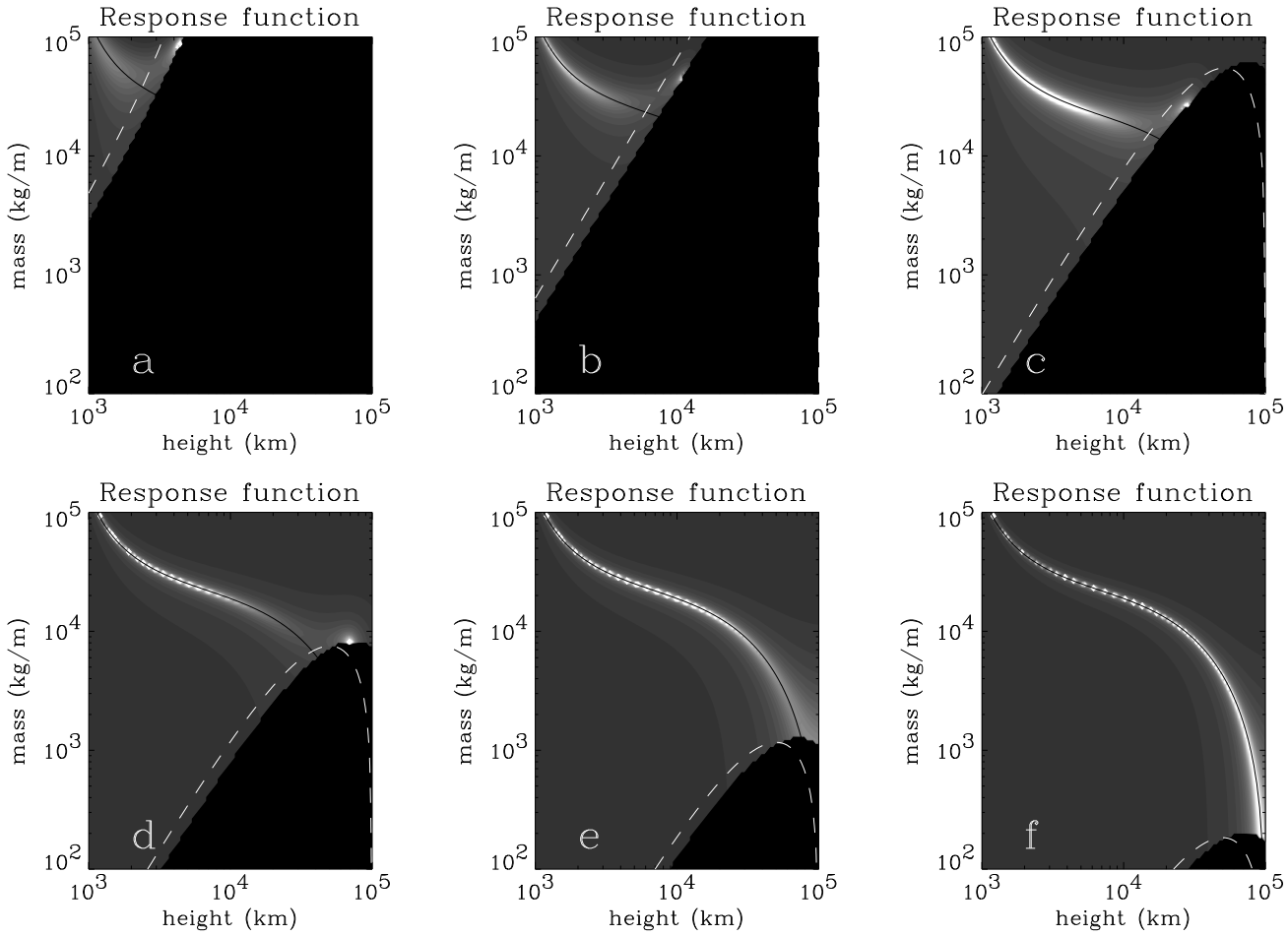

Fig. 9a–e. Grayscale plot of the response function of forced oscillations in IP prominences for driving periods of 5 min. The curved black line shows prominences whose quasi-stationary eigenperiods are equal to the forcing period. The dashed white line shows prominences with $\omega_{\rm stat}\tau_0 = 1$. The black area shows prominences that are unstable. The response function is plotted as a grayscale, with white denoting the largest response. The single white dot in some graphs, results from a prominence whose dynamical eigenperiod matches the driving period. The arcade field is $B_0 = 0.001$ T and $H = 100\,000$ km. **a** $v_{\rm A} = 100$ km/s; **b** $v_{\rm A} = 251$ km/s; **c** $v_{\rm A} = 631$ km/s; **d** $v_{\rm A} = 1\,585$ km/s; **e** $v_{\rm A} = 3\,981$ km/s; **f** $v_{\rm A} = 10\,000$ km/s.

4. Conclusions

In this Paper I made a comparative study of the vertical oscillations of both NP and IP prominences. More specific, I investigated the influence of an important boundary condition, photospheric flux conservation, on the stability of such oscillations. As the photosphere is a finite distance away from the main prominence body, a delay τ_0, comparable to the Alfvén crossing time, is introduced in the effect of this boundary condition. To my knowledge, this is the first attempt at comparing NP and IP prominences taking the dynamical field evolution into account.

Both NP and IP vertical prominence equilibria can globally be described by the same force balance (Eq. (1)) between gravity, the overlying arcade and the repelling influence of the photosphere (see also Priest 1990). The difference stems from the relative orientation of prominence current and coronal arcade field. This very basic force balance and the very simple prominence model I use (an infinitely long, infinitely thin current wire) nevertheless lead to the same topologies and equilibria found by other authors who used an MHD approach. In particular, the current in an IP prominence is usually one or two orders of magnitude larger than the one in a similar NP prominence (Démoulin & Priest 1988). Closely related to this, is the observation that global oscillation periods (derived from quasi-stationary theory) for IP prominences are much shorter than for NP prominences.

The model for vertical IP prominence dynamics, presented in Paper I, was extended to include the effects of gravity. Thus it became possible to use the same formalism to describe IP and NP prominences and to compare the effects of a delayed boundary condition on oscillating NP and IP prominences. The growth rates and periods of both NP and IP prominences were computed for a wide range of values for the delay τ_0. The results show that retardation is of little consequence for the oscillation of an NP prominence. The dominant forces in an NP equilibrium are resulting from gravity and the overlying magnetic arcade.

The photosphere plays only a minor role. In addition, the intrinsic time scales of NP prominences (e.g. the quasi-stationary period) are much larger than the typical delay time τ_0. Hence a quasi-stationary description suffices for NP filaments.

In contrast, the stability properties of IP prominences are strongly affected by retardation if $\omega_0\tau_0 \gtrsim 1$, where ω_0 is the oscillation frequency (usually the quasi-stationary frequency $\omega_{\rm stat}$ is a good enough approximation). If $\omega_0\tau_0 \approx 1$, the growth rate depends sensitively on τ_0. For increasing τ_0, the oscillation first becomes strongly damped and then looses stability. In particular, as τ_0 depends on the height of the filament, there is a range in heights at which oscillations are inhibited. At slightly larger heights a prominence will become unstable. Depending on the actual parameter values, this instability can set in at lower heights than the quasi-stationary van Tend-Kuperus instability (van Tend & Kuperus 1978). Also, externally driving the system is most efficient when the driving frequency $\omega_{\rm d}$ matches the free oscillation frequency ω_0 *and* the resonance condition is met: $\omega_0\tau_0 \approx 1$. These conditions may lead to a diagnostic tool for the physical parameters of the prominence equilibrium. In Paper I, I showed that the effects of retardation were due to the delayed photospheric repelling force being either in phase or anti-phase with the actual oscillation (constructive/destructive interference).

The results of this paper can be used to obtain information about the physical conditions prevailing in filaments. The oscillation periods derived in the quasi-stationary limit are usually a good approximation to the periods found using the dynamically self-consistent approach employed in this paper. This could not have been foreseen a priori, since the delay τ_0 introduces a new timescale, usually quite different from the quasi-stationary period. Consequentially, Fig. 3 suggests that the long period oscillations (30–60 min.) sometimes observed in prominences, exclude an IP field topology. Even though our results pertain to global oscillations, this is likely to be true in general, as higher mode oscillations usually have smaller periods. If one can estimate the magnitude of the coronal background field (e.g. from magnetogram data and force-free field extrapolations) and the height of a prominence (from observations on the limb), it is possible to determine the filament current I_0. This, combined with the observed oscillation period, can be used to derive the mass density per unit length m of the prominence. If one also has information on the damping rate of the oscillation, it is possible to derive an average delay τ_0 (and hence Alfvénspeed $v_{\rm A}$) for waves travelling between prominence and photosphere.

One can also apply the results to a statistical study of prominences, thereby excluding the need for detailed information like field strengths and filament heights. IP prominences should show, on average, smaller quality factors (if $\nu_{\rm ph} = 0$) than NP prominences, due to retardation effects. If $\nu_{\rm ph} \neq 0$ (as can be expected), the typical height dependence of the quality factor (see curve b_1 in Fig. 8) can still be used to distinguish retardation from damping mechanisms like mass friction or wave emission that occur in both types of prominences.

Acknowledgements. The author is financially supported by the Netherlands Organisation for Scientific Research (NWO) under grant nr. 781-71-047. The author gratefully acknowledges stimulating discussions with Max Kuperus and Bert van den Oord. The author thanks the referee, dr. J.-M. Malherbe, for his useful comments.

References

Abramowitz M., Stegun I. (eds), 1968, Handbook of Mathematical Functions, Dover Publications
Amari T., Aly J.J., 1989, A&A 208, 261
Anzer U., Ballester J.L., 1990, A&A 238, 365
Balthasar H., Wiehr E., Schleicher H., Wöhl H., 1993, A&A 277, 635
Démoulin P., Priest E.R., 1988, A&A 206, 336
Démoulin P., Priest E.R., Ferreira J., 1991, A&A 245, 289
Drake J.F., Mok Y., van Hoven G., 1993, ApJ 413, 416
Hyder C.L., 1966, Z. Astrophys. 63, 78
Joarder P.S., Roberts B., 1992, A&A 261, 625
Joarder P.S., Roberts B., 1993, A&A 277,225
Joarder P.S., Nakariakov V.M., Roberts B., 1997, submitted
Kaastra J., 1985, Solar flares, an elecrodynamical model, thesis University Utrecht, the Netherlands
Kippenhahn R., Slüter A., 1957, Z. Astrophys. 43, 36
Kleczek J., Kuperus M., 1969, Sol. Phys. 6, 72
Kuperus M., Raadu M.A., 1974, A&A 31, 189
Leroy J.L., Bommier V., Sahal-Bréchot S., 1984, A&A 131, 33
Martens P.C.H., Kuin N.P.M., 1989, Sol. Phys. 122, 263
Morse P.M., Feshbach H., 1953, Methods of Theoretical Physics, McGraw-Hill Book Company, inc.
Oliver R., Ballester J.L., 1995, ApJ 448, 444
Oliver R., Ballester J.L., 1996, ApJ 456, 393
Oliver R., Ballester J.L., Hood A. W., Priest E. R., 1992, ApJ 400, 369
Oliver R., Ballester J.L., Hood A. W., Priest E. R., 1993, ApJ 409, 809
Priest E.R., 1990, Dynamics of quiescent prominences, Springer-Verlag, Eds. Ruždjak, V., Tandberg-Hanssen, E.
Ramsey H.E.,Smith S.F., 1966, AJ 71, 197
Ridgway C., Amari T., Priest E.R., ApJ 378, 773
Saaty Th.L., 1981, Modern Nonlinear Equations, Dover Publications
Schmieder B., 1988, Dynamics and Structures of Quiescent Solar Prominences, Ch. 2, Kluwer Academic Publishers, Ed. Priest, E.R.
Schmieder B., 1992, Sol. Phys. 141, 275
Schutgens N.A.J., 1997, A&A in press, (Paper I)
Thompson W.T., Schmieder B., 1991, A&A 243, 501
Tsubaki T., 1988, Proc. Sacramento Peak summer Workshop, p. 140, Ed. Altrock, R.C.
van den Oord G.H.J., Kuperus M., 1992, Sol. Phys. 142, 113
van Tend W., Kuperus M., 1978, Sol. Phys. 59, 115
Vrsnak B., Ruzdjak V., 1994, Solar Coronal Structures, IAU Coll. 144, Eds. Rusin V., Heinzel P., Vial J.-C.
Yi Zhang, Engvold O., 1991, Sol. Phys. 134, 275
Yi Zhang, Engvold O., Keil S.L., 1991, Sol. Phys. 132, 63

This article was processed by the author using Springer-Verlag LaTeX A&A style file *L-AA* version 3.